IEEE Access
Multidisciplinary | Rapid Review | Open Access Journal

Received May 28, 2019, accepted June 10, 2019, date of publication June 26, 2019, date of current version July 15, 2019.

Digital Object Identifier 10.1109/ACCESS.2019.2925146

Comprehensive Design Methodology of Compound-Split Hybrid Electric Vehicles: Introduction of the Compound Lever as a Design Tool

HYUNJUN KIM, TOUMADHER BARHOUMI, AND DONGSUK KUM, (Member, IEEE)
Korea Advanced Institute of Science and Technology, Daejeon 34141, South Korea

Corresponding author: Dongsuk Kum (dskum@kaist.ac.kr)

This work was supported in part by the National Research Foundation of Korea (NRF) under Grant NRF-2017R1C1B2009110, and in part by the Technology Innovation Program (10051876, Development of novel power-train configurations for power-split (P)HEVs with world-class fuel economy and acceleration performance).

ABSTRACT Powertrain configurations described with elementary (physical) levers can intuitively depict the connections between planetary gear (PG) shafts and powertrain components. However, finding optimal compound-split hybrid configurations using the elementary lever is practically impossible due to the large design space. In fact, each of the existing 252 compound-split configurations has three design variables: two PG gear ratios and a final drive gear ratio. In this paper, a compound (virtual) lever-based design methodology that eliminates redundant elementary lever designs is proposed to enable a full compound-split hybrid electric vehicles design domain search. The performance metrics were assessed in the compound lever design space. Later, the designs were converted back to elementary lever configurations by applying a design space conversion map, and their performance metrics were plotted on a fuel economy versus acceleration performance plane to compare the potential of the 252 compound-split configurations. Finally, an optimal configuration that can reach 0-160 kph in 15.36 sec, which is 5.90 sec faster than that of the Prius configuration, while maintaining a competitive fuel economy, was selected. The proposed method revealed that there are still many configurations that are potentially better than the commercially available split hybrids.

INDEX TERMS Compound lever, compound-split, design methodology, multi-objective configuration selection, power-split hybrid electric vehicle.

I. INTRODUCTION

Power-split hybrids, in which the transmission is replaced by electric machines (or motor/generators) and a power split device (e.g. planetary gear set (PG)), are suitable for both hybrid electric vehicles (HEV) and plug-in HEV because they provide high traction power for the electric vehicle (EV) mode and can potentially achieve high acceleration performance as well as good fuel economy if the system is properly designed [1]. However, finding the best split HEV configuration and realizing the full potential of the given components are non-trivial problems due to the large design space. As illustrated in Table 1, there exist many split HEV configurations depending on the connections between the powertrain components (engine, electric machines, and output shaft) and the PG(s) shafts (sun, ring, and carrier). For instance, connecting two PGs through two common shafts results in 252 compound-split configurations [2].

In order to find the best configuration, performance metrics such as the fuel economy (FE) and acceleration performance (AP) must be evaluated for each of these configurations. Furthermore, the sun/ring gear ratios (SR_{ratio}) and the final drive ratio (FD_{ratio}) should be considered as design variables to assess the full potential of these configurations as the performance of a given configuration changes depending on its design variables [3], [4]. Unfortunately, evaluating the FE and AP across the entire design space is practically impossible due to the high computational load of the adopted

The associate editor coordinating the review of this manuscript and approving it for publication was Ahmad Elkhateb.

optimal control algorithms such as dynamic programming, which guarantees the full potential of each design [5], [6]. In order to resolve this high computational load problem, prior studies have adopted either configuration-screening approaches or iterative optimization approaches when searching for the best split HEV configurations.

In the screening approach, configurations are preliminarily sorted before evaluating their performance metrics to reduce the number of feasible configurations (e.g. [7]–[9]). For instance, Conlon compared the transmission efficiencies of three compound-split configurations that were considered to be useful [10]. Similarly, another study by Wang *et al.* adopted the compound lever to analyze the performance of compound-split configurations based on the characteristics of the mechanical points and the components' torque and speed relationships [11]. However, the optimality of the selected configurations cannot be guaranteed since most of the configurations were excluded in both studies based on engineering intuition or simple static analysis results. Other studies applied the optimization theory to a few candidates that were selected based on several screening criteria (e.g. [12]–[16]). For instance, Liu *et al.* and Li *et al.* tried to reduce the computational burden by filtering out many configurations based on their launching performance criteria when selecting optimal split HEV configurations with two PG [17], [18]. Recent studies have adopted a similar approach to solve the design problem of multi-mode power-split hybrids using two and three PGs [19]–[21]. Configurations with poor launching performance were screened out and the performance of feasible configurations was evaluated using the power-weighted efficiency analysis for rapid sizing (PEARS) tool [22]. However, the screening processes proposed in all these studies are based on the physical design space, which implies that redundant configurations are evaluated as discussed in [2]. More importantly, such approaches do not provide any insight into how the performance metrics change when the configuration or design variables vary.

In the iterative optimization approach, optimization algorithms were applied to a relatively large design space. Ahn *et al.* used a parameter optimization program to find the optimal compound lever design while setting the fuel economy as the cost function [23]. However, the insight into how to design split hybrid configurations is insufficiently provided because the convex optimization does not fully explore the compound-split HEV design space. Furthermore, the physical feasibility of the selected design cannot be guaranteed since the optimization process was done in the nonphysical (compound lever) design space. On the other hand, Bayrak *et al.* enumerated two PGs configurations in the physical design space using the graph theory and iteratively compared the fuel economy to select optimal configurations [4], [24]. However, these approaches used either a static analysis (e.g. transmission efficiency) or a suboptimal trajectory optimization algorithm to reduce the computational load. In summary, previous design methodologies either investigated as part of the entire design space by filtering out candidates and/or using fast performance evaluation techniques, and thus, these approaches can neither guarantee the global optimality of the configurations nor provide any insight into the design of optimal compound-split configurations.

In this paper, a comprehensive design method that fully searches the entire design space with a minimum computational burden is proposed in order to find new outstanding compound-split HEV configurations and to provide useful insight and guidelines to designers. The main contribution of this study is adopting the virtual design space to efficiently assess the performance metrics of compound-split hybrids and select optimal virtual designs. Thanks to using the virtual design space, which maps all the separate design spaces of each physical topology onto a single continuous design space, the redundancy existing within the physical design space is omitted. Solving the compound-split HEVs design problem in such a manner implies that there is no need to compromise on the optimizer as the design space was dramatically reduced. It also provides insights on the overall performance trends throughout the entire compound-split HEV design space. For a systematic comparison of the many compound-split hybrid configurations, the selected virtual designs are converted back to physical designs using the design space conversion methodology introduced in [2].

The remainder of this paper is organized as follows. In section II, the two different design spaces of compound-split HEVs are introduced and their relationships are discussed to describe the main idea of the proposed optimal configuration selection methodology. Section III describes the problem formulations for the evaluation of fuel economy and acceleration performance within the compound lever design space. The simulation results are also presented and analyzed in this section. In Section IV, compound lever designs are converted back to 252 compound-split configurations using the design space conversion map, and the performance metrics are compared to systematically select the optimal compound-split configurations. Finally, section V includes the concluding remarks.

II. DESIGN SPACE OF THE COMPOUND-SPLIT HYBRID ELECTRIC VEHICLE

In this section, the two different design spaces of compound split HEVs are introduced, and the relationships between these two design spaces are elucidated. Then, the main idea of the compound lever based design methodology is described.

A. ELEMENTARY LEVER DESIGN SPACE

The lever analogy was introduced in the 1980s to help the analysis and design of automatic transmissions [25]. Later on, it was adopted to visualize and analyze the dynamic behaviors of power-split HEVs (e.g. [7]–[13]). In this study, an elementary lever refers to a three-node lever, which represents the PG. Each node on the elementary lever corresponds to each PG shaft (i.e. ring, carrier, and sun gears).

TABLE 1. Classification of single and double planetary gear (pg) split hybrid powertrains.

Number of PGs	1	2	
Classification	Input or Output-split	Input or Output-split	Compound-split
Number of Configurations	24	432	252
Example of Configurations		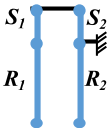	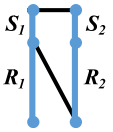
Design Variables	SR_{ratio} FD_{ratio}	$SR_{1,ratio}$,$SR_{2,ratio}$ FD_{ratio}	$SR_{1,ratio}$,$SR_{2,ratio}$ FD_{ratio}

Since the elementary lever retains the nodes' physical information, the multiple PG configurations described by elementary levers can depict the physical connections between the PG shafts (See Table 2). These connections, as well as the components arrangement, play an important role in calculating how many compound-split configurations exist. There is a total of 21 different ways of connecting two PGs: twelve 2PG arrangements (i.e. #1 …#12 illustrated in Appendix A) and nine reversed 2PG arrangements (i.e. #1r …#11r illustrated in Appendix A where 'r' represents the reversed arrangement) [2]. Note that the three reversed 2PG arrangements #2r, #8r, and #12r are identical to #2, #8, and #12, respectively, and are thus omitted.

For the components arrangements, there are twelve different ways to arrange the four powertrain components (i.e. engine, two electric machines (EM A and EM B), and output shaft) on a four-node lever (i.e. compound lever). These twelve components arrangements are defined as C1, C2, C2, C3, C4, C5, C6, C1s, C2s, C3s, C4s, C5s, and C6s, where "s" represents the switched location of EM A and EM B. Note that reversed components arrangements are not taken into account because the operating characteristics and performance of the reversed cases are the same as those of the original ones. By listing all the combinations of these 12 components arrangements and 21 PG arrangements, 252 compound-split configurations can be generated as illustrated in Table 2. The name of each configuration is determined simply by adding the two naming schemes of the PG and components arrangements (e.g. Configuration #1-C1 is obtained when combining the components arrangement C1 in Appendix B and the PG arrangement #1 in Appendix A).

The design space of each of the 252 compound-split HEV configurations built as illustrated in Table 2 is composed of three design variables: the SR_{ratio} of the first and second PGs (i.e. SR_1 and SR_2, respectively) and FD_{ratio}. Since these design variables have substantial impacts on the performance of a given configuration, the performance metrics of the

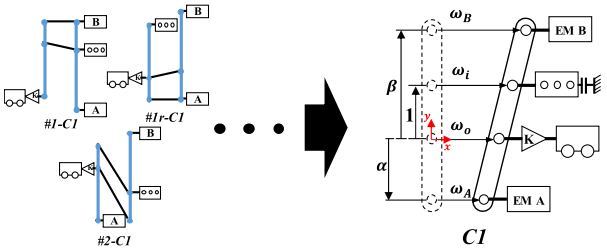

FIGURE 1. Compound lever representation of compound-split HEVs.

TABLE 2. 252 elementary lever configurations of compound-split hev.

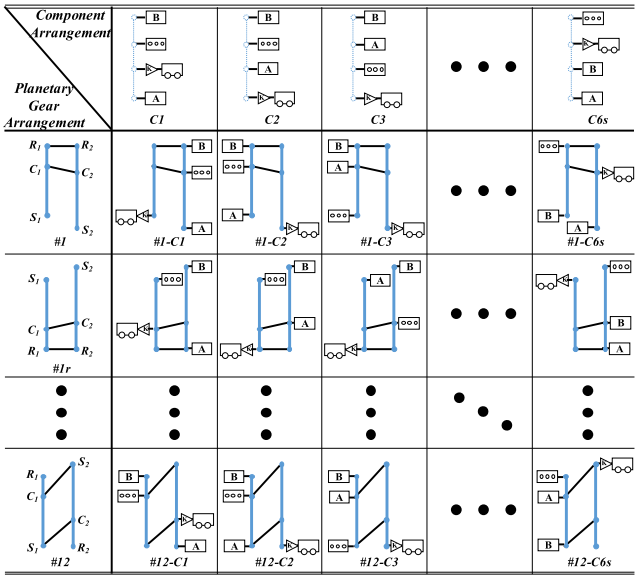

252 compound-split configurations must be thoroughly evaluated across the entire design space. However, evaluating the performance of all the elementary lever designs is practically impossible due to the heavy computational load. Thus, when searching for optimal compound-split configurations, an alternative tool is needed to enable the full design domain search with a minimum calculation effort.

B. COMPOUND LEVER DESIGN SPACE

The compound lever is a virtual lever that depicts only the positions of the two electric machines relative to the position of the engine with respect to that of the vehicle. Originally, the compound lever was proposed to simplify the connected elementary lever configurations [25]. When a split HEV configuration is represented with a compound lever, connections between the PGs are omitted. Instead, the relative locations of the powertrain components are explicitly illustrated on a single compound lever. Despite incurring a loss of information, the unified characteristic of the compound lever can play a key role in the performance assessment and the design of a compound-split HEV as redundant designs are completely eliminated in the compound lever space.

While many prior studies used the graph theory to enumerate all existing power-split configurations (e.g. [26], [27]), all possible compound-split configurations can also be

TABLE 3. 12 Sub-groups of the compound lever.

$\beta > 1$	C1	Input (i1 & i2)	C2 / C3 / C3s	Output (o1 & o2)	
$\beta = 1$	Output-split (o6s & o5s)	X	Output-split (o4s & o3s)	X	Output-split (o2s & o1s)
$0 < \beta < 1$	C4	Input (i3 & i4)	C5 / C5s	Output (o3 & o4)	C2s
$\beta = 0$	Input-split (i6s & i5s)	X	Input-split (i4s & i3s)	X	Input-split (i2s & i1s)
$\beta < 0$	C6 / C6s	Input (i5 & i6)	C4s	Output (o5 & o6)	C1s
β / α	$\alpha < 0$	$\alpha = 0$	$0 < \alpha < 1$	$\alpha = 1$	$\alpha > 1$

systematically defined using the compound lever [10]. In fact, the compound lever can describe all 252 elementary lever configurations, and there is a clear relationship between the two design spaces as discussed in [2]. Depending on the components arrangements, the compound lever can be classified into 12 different sub-groups, each of which can be superimposed on the 21 PG arrangements, resulting in 252 compound-split configurations. Although the design space of the compound lever is divided into 12 different sectors as illustrated in Table 3, all compound lever designs can be represented with a single compound lever using two design variables, α and β, which represent the normalized distances between the vehicle node and the electric machines' nodes. Therefore, the performance trend of all the compound-split HEV configurations can be observed in one continuous design space without any redundancy. This helps engineers understand how the components arrangements affect the performance of compound-split HEVs throughout the whole design space, and thus, provides a guide for the design of optimal compound-spilt HEV configurations.

C. DESIGN SPACE CONVERSION MAP

The compound lever design space inherently does not have any redundancy, and thus, evaluating the performance metrics within the compound lever design space dramatically reduces the computational load. However, its design variables, α and β, do not have any physical significance, and must be converted into physical compound-split designs (i.e. elementary lever configurations) and the two SR_{ratio}s. Therefore, a design space conversion map enabling the inter-conversion between the compound lever and the elementary lever design spaces is introduced.

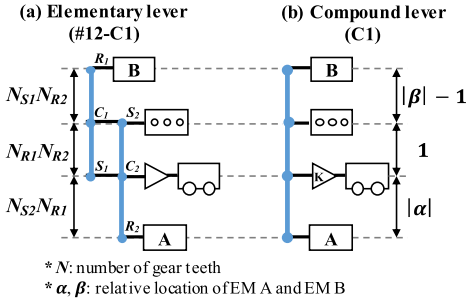

FIGURE 2. Relationship between elementary lever and compound lever (e.g. #12-C1).

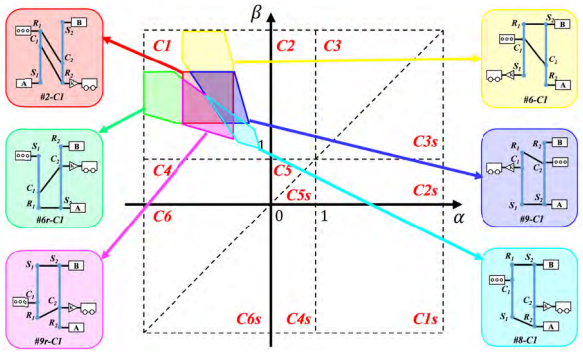

FIGURE 3. Conversion map of configurations #2-C1, #6-C1, #6r-C1, #8-C1, #9-C1, and #9r-C1 illustrated in region C1. Note that the feasible SR_{ratio} range is assumed to be between 0.3 and 0.7.

The design space conversion map is extracted from the relationship between the elementary lever design variables (i.e. N_{S1}, N_{R1}, N_{S2}, and N_{R2}, which are the number of the sun and ring gear teeth numbers of the two PGs) and compound lever design variables (i.e. α, β). As observed in Fig. 2, the PG arrangement #12 and the virtual compound lever C1 are compared, and the following equation is derived.

$$N_{S1}N_{R1} : N_{R1}N_{R2} : N_{S2}N_{R1} = \beta - 1 : 1 : -\alpha. \tag{1}$$

By solving Eq. (1), the conversion equations are obtained as follows:

$$\alpha = -\frac{N_{S2}N_{R1}}{N_{R1}N_{R2}} = -SR_2 \tag{2}$$

$$\beta = \frac{N_{S1}N_{R2}}{N_{R1}N_{R2}} + 1 = SR_1 + 1. \tag{3}$$

By repeating this process for each of the other PG arrangements illustrated in Appendix A, the design space conversion map is derived. An example of the conversion map of C1 is illustrated in Fig. 3. As observed in Fig. 3, the compound lever and the elementary lever have a one-to-N relationship. For example, the compound lever design with $\alpha = -2$ and $\beta = 3$ can be converted into six different configurations. On the other hand, the design with $\alpha = -4.5$ and $\beta = 3$ can only be converted into one configuration (i.e. #6r-C1). This means that the performance metrics of the physical compound-split configurations do not need to be repeatedly evaluated. Therefore, this study proposes to conduct a full design domain search in the compound lever space, and then evaluate the

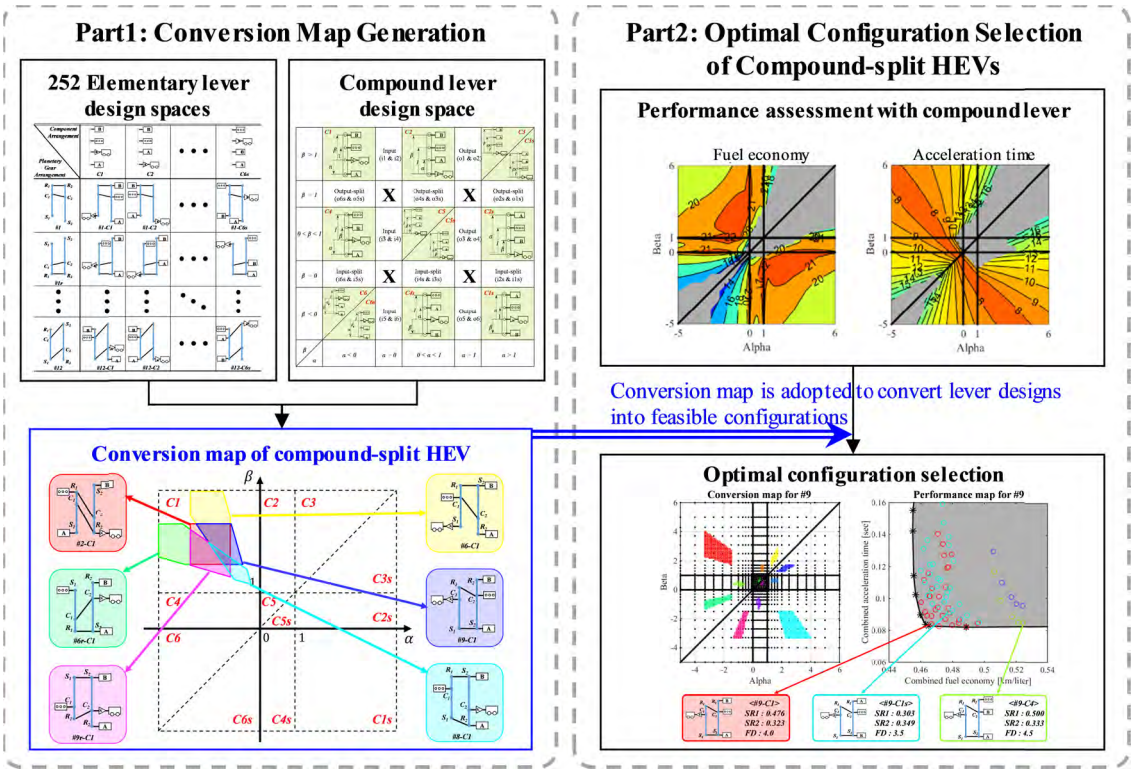

FIGURE 4. Overview of the design methodology.

full potential of each configuration using the design space conversion map. The reader is encouraged to read [2] for more details about the conversion maps generation process.

D. COMPOUND LEVER BASED DESIGN METHOD

The compound lever based optimal configuration search methodology consists of two steps: 1) performance assessment and 2) optimal configuration selection, as shown in Fig. 4. First, to reduce the computational load by eliminating the redundant physical designs, the fuel economy and the acceleration performance of compound-split HEVs are evaluated in the compound lever design space. Second, to compare the full potential of each configuration, the performance metrics are plotted onto a 'fuel economy- acceleration performance' plane. Then, the design space conversion map is used to convert compound lever designs to elementary lever configurations. Finally, an optimal compound-split configuration is selected and compared with other configurations as described in Fig. 4.

III. PERFORMANCE ASSESSMENT IN THE COMPOUND LEVER DESIGN SPACE

In this study, the fuel economy and drivability potential of all compound-split HEVs are evaluated using dynamic programming (DP) within the compound lever design space, which consists of α, β, and FD_{ratio}. In subsection A, simulation settings such as the design grid of the compound lever, vehicle and components specifications, and DP problem formulations are defined. In subsections B and C, the performance assessment results for fuel economy and acceleration performance are discussed.

A. SIMULATION SETTINGS FOR PERFORMANCE ASSESSMENT

1) DYNAMIC EQUATIONS OF THE COMPOUND LEVER

Euler form dynamic equation of split HEVs, which was proposed and experimentally validated by Huei Peng's research group [28], [29], was adopted by many prior studies and showed trustful results. Thus, the dynamic equation of the virtual compound lever illustrated in Fig. 1, which adopts the Euler form, is derived as follows:

$$\begin{bmatrix} \dot{\omega}_i \\ \dot{\omega}_o \\ \dot{\omega}_A \\ \dot{\omega}_B \end{bmatrix} = I_{\alpha\beta}^{-1} \begin{bmatrix} T_i + \alpha T_A + \beta T_B \\ -T_{load} + (1-\alpha) T_A + (1-\beta) T_B \\ 0 \\ 0 \end{bmatrix} \tag{4}$$

$$\text{with } I_{\alpha\beta}^{-1} = \begin{bmatrix} I_i & 0 & \alpha I_A & \beta I_B \\ 0 & I_m & (1-\alpha) I_A & (1-\beta) I_B \\ -\alpha & (\alpha-1) & 1 & 0 \\ -\beta & (\beta-1) & 0 & 1 \end{bmatrix},$$

where I_i, I_A, and I_B and T_i, T_A, and T_B are the inertias and torques of the engine, EM A, and EM B, respectively. The road load torque T_{load} is defined as follows:

$$T_{load} = \frac{r}{K} \left(f_0 + f_1 v + f_2 v^2 \right), \tag{5}$$

TABLE 4. Vehicle and components specifications for design search [30]–[32].

Component	Parameter	Value
Vehicle	Mass (m)	1530.87 kg
	Coast-down Coefficients	f_0=82.32, f_1=0.22, f_2=0.40
	Wheel Radius (r)	0.305 m
Engine	Inertia (I_i)	0.18 kg · m^2
	Speed ($\omega_{i,max}$)	5200 RPM
	Torque ($T_{i,max}$)	142Nm @ 4000 RPM
	Power ($P_{i,max}$)	73kW @ 5200 RPM
EM A	Inertia (I_A)	0.0226 kg · m^2
	Speed ($\omega_{A,max}$)	13500 RPM
	Torque ($T_{A,max}$)	207 Nm @ [0:3000] RPM
	Power ($P_{A,max}$)	60 kW @ 3000 RPM
EM B	Inertia (I_B)	0.0087 kg · m^2
	Speed ($\omega_{B,max}$)	13500 RPM
	Torque ($T_{B,max}$)	170 Nm @ [0:2247] RPM
	Power ($P_{B,max}$)	40 kW @ 2985 RPM

where r and K refer to the wheel radius and the final drive ratio, respectively, and f_0, f_1, and f_2 are the coast-down coefficients. Both the fuel economy and the acceleration performance of all the compound-split HEV designs are evaluated by adjusting α, β, and K in Eq. (4). Note that during the EV mode, the engine speed is fixed to zero by engaging the engine brake.

2) VEHICLE AND COMPONENTS SPECIFICATIONS

In this study, the components and vehicle specifications of the Prius 3rd generation were used for the performance assessment (See Table 4). The vehicle mass and coast-down coefficients were adopted from the "Downloadable Dynamometer Database (D^3)" published by Argonne National Laboratory [30]. The specifications and efficiency maps of the engine and EM A were extracted from a research paper published by Toyota [31], [32]. The specifications of EM B, however, were not available, and thus, were estimated assuming that the peak speed of EM B is the same as that of EM A, and that the maximum torque and power of EM B are about 82% and 67% of those of EM A, respectively.

3) POINTS OF INTEREST IN THE COMPOUND LEVER DESIGN SPACE

Before selecting the points of interest (i.e. the design grid), the ranges of the two design variables, α and β, were bounded between -5 and 6 in order to cover a finite but sufficiently large design space. The points of interest (POI) were selected such as each configuration is given a fair opportunity. The input-split ($\alpha = 0$ or $\beta = 0$) and output-split ($\alpha = 1$ or $\beta = 1$) configurations are not compound-split designs, but their performance metrics were also assessed to gain insight into the performance of various types of split HEVs. The number of POIs per single $\mathrm{FD_{ratio}}$ is 33*33 = 1,089, and thus, the fuel economy and the acceleration performance

TABLE 5. Dp problem formulation for the fuel economy and acceleration performance assessment.

Design space	$\alpha, \beta: -5:6$ FD_{ratio} : [2.5, 3.0, 3.5, 4.0, 4.5]	
Cost	Fuel consumption (gram)	Time (sec)
Stage	Time of driving cycle (UDDS, HWFET)	Velocity: [0:1:160] (km/h)
Control	T_e: $[0{:}\frac{T_{e,max}}{50}{:}\ T_{e,max}]$ ω_e:$[\omega_{e,min}{:}\frac{\omega_{e,max}-\omega_{e,min}}{50}{:}\ \omega_{e,max}]$	T_e: $[0{:}\frac{T_{e,max}}{50}{:}\ T_{e,max}]$ T_A: $[-T_{A,max}{:}\frac{T_{1,max}}{20}{:}\ T_{\mathrm{A},max}]$ T_B: $[-T_{\mathrm{B},max}{:}\ \frac{T_{2,max}}{20}{:}\ T_{\mathrm{B},max}]$
State	SOC: [0.4:0.001:0.8]	ω_e: $[\omega_{e,min}{:}\ \frac{\omega_{e,max}-\omega_{e,min}}{40}{:}\ \omega_{e,max}]$
Subject to	$\mathrm{SOC_{initial}} = SOC_{final}$, $0.4 \le \mathrm{SOC} \le 0.8$ (only for FE assessment) $w_{e,min} \le w_e \le w_{e,max}$, $0 \le T_e \le T_{e,max}(w_e)$ $-w_{\mathrm{A},max} \le w_{\mathrm{A}} \le w_{\mathrm{A},max}$, $-T_{\mathrm{A},max}(w_{\mathrm{A}}) \le T_{\mathrm{A}} \le T_{\mathrm{A},max}(w_{\mathrm{A}})$ $-w_{\mathrm{B},max} \le w_{\mathrm{B}} \le w_{\mathrm{B},max}$, $-T_{\mathrm{B},max}(w_{\mathrm{B}}) \le T_{\mathrm{B}} \le T_{\mathrm{B},max}(w_{\mathrm{B}})$	

are assessed for the total number of 5,445 POIs ($\mathrm{FD_{ratio}} = 2.5 : 0.5 : 4.5$) to find optimal compound-split configurations. This is a dramatically reduced number compared to the 31,500 POIs ($\mathrm{SR_{ratio1/2}} = 0.3 : 0.1 : 0.7$, $\mathrm{FD_{ratio}} = 2.5 : 0.5 : 4.5$ for each of 252 configurations) of the elementary lever design space.

4) DYNAMIC PROGRAMMING FORMULATION

In order to fairly compare the configurations, a control strategy must be optimized to compute the fuel economy and acceleration performance potentials of each design. In this study, two performance metrics are computed using dynamic programming (DP). Formulating DP problems is complicated but DP guarantees global optimality and thus, is widely used for the performance assessment of HEVs [5], [6]. In Table 5, the fuel economy (FE) and acceleration performance (AP) DPs are defined, and the cost, stage, control, state variables, and constraints are summarized for each DP problem [6], [7], [33]. Note that both the FE and AP DP problems were solved for all POIs, and their results are provided in the following sections. The FE is evaluated for urban dynamometer driving schedule (UDDS) and highway fuel economy driving schedule (HWFET) as these two cycles are the standard driving cycles of many countries such as U.S. and Republic of Korea.

B. FUEL ECONOMY ASSESSMENT RESULTS

City and highway FEs were evaluated for 5,445 compound lever designs using six i7-4790K CPU @ 4.00GHz, 8GB RAM computers. The calculation took about 81 hours per computer when four Matlab codes were run in parallel by each computer. Note that if the FE is assessed using near-optimal algorithms, the calculation time can be reduced [34], [35]. However, in this study, DP, which is computationally heavy but guarantees finding the global

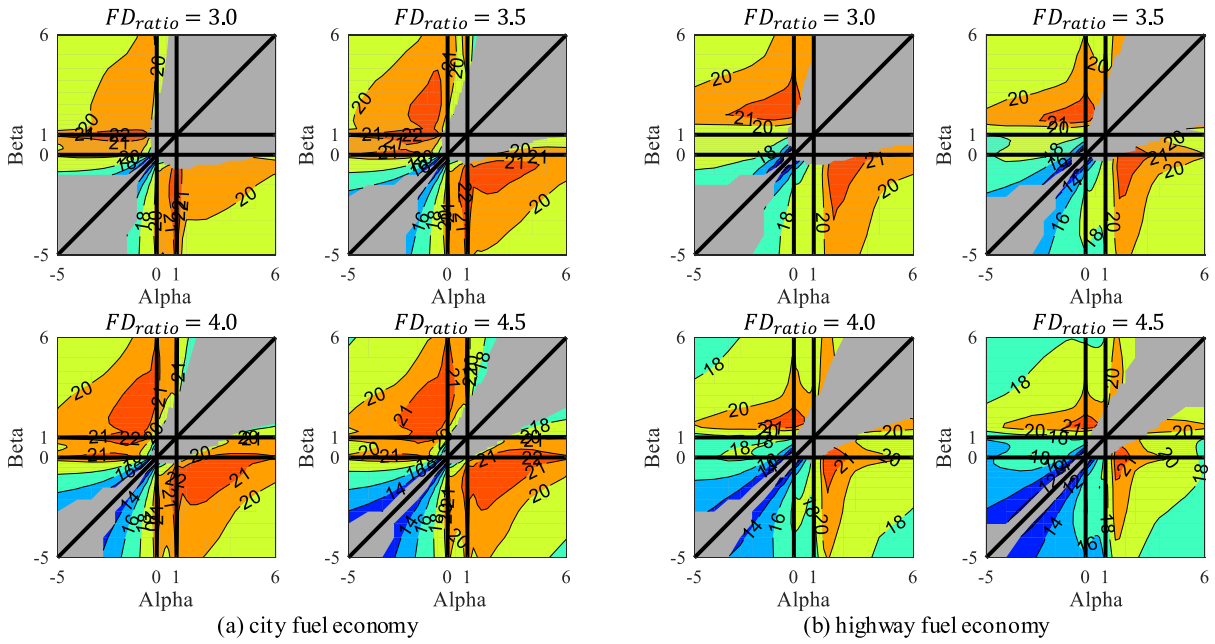

FIGURE 5. City and highway fuel economies contours of the compound lever design space.

optimum, was adopted because the full compound-split HEV design space was assessed for the very first time.

The FE results were plotted on the compound lever design space as shown in Fig. 5. The four contour maps in Fig. 5(a) show the city FE for the four selected FD_{ratio}s (3, 3.5, 4, and 4.5); the four contour maps in Fig. 5(b) correspond to the highway FE for the same FD_{ratio}s. Note that the gray regions in Fig. 5 represent infeasible designs that cannot meet the torque, speed, or power demands of the given driving cycle. As observed in Fig. 5 (a), not only the compound-split designs but also the input- and output-split designs achieved high FE during the city driving cycle. On the other hand, the input-split and compound-split designs (i.e. regions C1 and C1s in Fig. 5 (b)) show high FE for the highway driving cycle. In order to find the optimal design that guarantees high FE across a wide range of vehicle speeds, the combined FE was calculated as follows:

$$FE_{combined} = \frac{1}{\frac{p}{FE_{UDDS}} + \frac{(1-p)}{FE_{HWEFT}}}, \tag{6}$$

where FE_{UDDS}, FE_{HWEFT}, and $FE_{combined}$ refer to city, highway, and combined FEs, respectively. Note that the weighting factor p was set as 0.45 based on the U.S. Federal FE testing [36]. In the combined FE results, the FE of regions C1 (i.e. $\alpha < 0, \beta > 1$) and C1s (i.e. $\alpha > 1, \beta < 0$) are higher than those of other regions (i.e. C2-C6 and C2s-C6s). This implies that the FE is optimal in regions C1 and C1s, which suggests locating the engine and output nodes between those of the two EMs in the compound levers (See Table 3). From the gray areas in the regions C3, C3s, C6, and C6s, one can conclude that locating the EMs in the same side of the lever leads to an infeasible powertrain. However, it is too early to conclude that C1 and C1s are optimal levers because their acceleration performance may be not acceptable. Therefore, both FE and AP must be simultaneously considered when selecting an optimal configuration.

C. ACCELERATION PERFORMANCE ASSESSMENT RESULTS

For the AP, the optimal torque trajectories of the engine, EM A, and EM B are determined to minimize the 0-160 km/h time for all compound lever designs. This optimization process took 97 hours with the same computing power that was used for the FE assessment. The 0-160 km/h time is decomposed into 0-100 km/h and 100-160 km/h acceleration times, which correspond to the low speed and high speed times, respectively. Figures 6 (a) and (b) illustrate the contours of the 0-100 km/h and 100-160 km/h times, respectively, obtained for four FD_{ratio}s. Similar to the FE results, the gray region corresponds to infeasible designs that could not reach 160 km/h or poor designs that required more than 30 second to reach 160 km/h.

Fig. 6 reveals that the regions C1, C1s, C4, C4s, C6, and C6s outperform other levers in terms of the AP, which is different from the FE results. One thing these six levers have in common is that the vehicle output drive node in each of them is located between the other three components (i.e. engine, EM A, and EM B) nodes in the compound lever (See Table 3). Such an arrangement enables the three powertrain components (i.e. engine, EM A, and EM B) to propel the vehicle. In other words, all three components can, if needed, provide motoring (positive) power rather than generating (negative) power. In fact, the best designs with minimum 0-100km/h times appear along the diagonal line from the top-left to the lower-right, where the utilization of the three

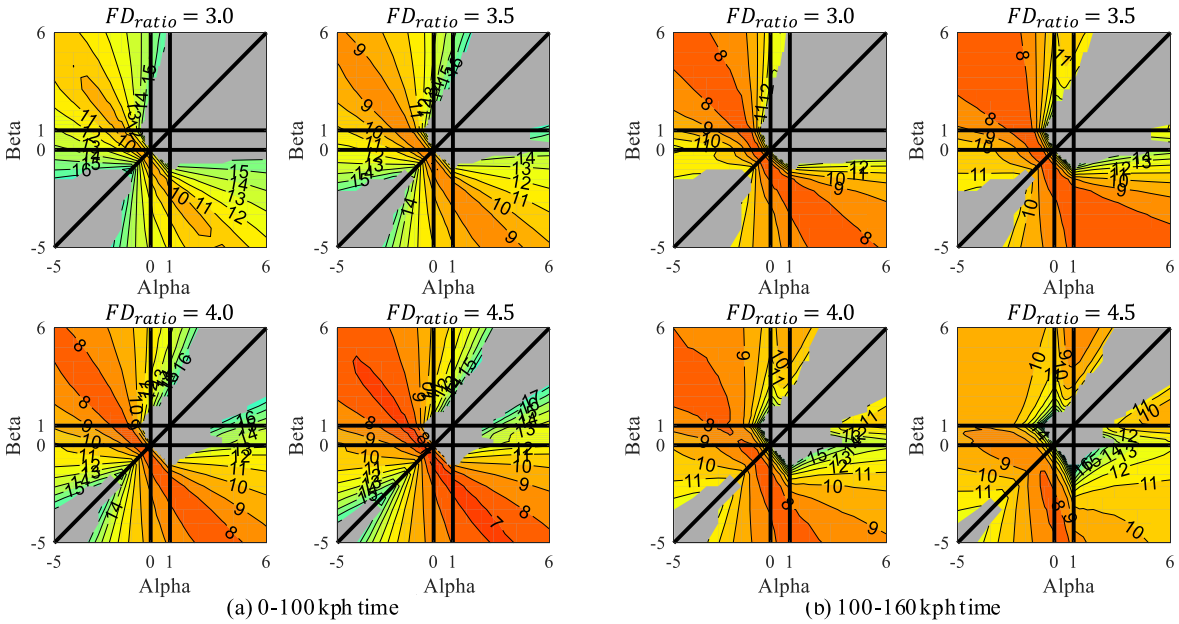

FIGURE 6. 0 – 100 kph time and 100 – 160 kph time contours of the compound lever design space (unit: sec).

power components is maximized. On the other hand, locating the vehicle output node at the end of the compound lever (e.g. regions C2, C2s, C3, C3s, C5s, and C5s) results in poor AP. The same tendency is also observed in the combined acceleration time contour, where the combined acceleration time is calculated using the following equation:

$$AT_{combined} = qAT_{0-100} + (2-q)\,AT_{100-160}, \tag{7}$$

where AT_{0-100}, $AT_{100-160}$, and $AT_{combined}$ represent the 0-100 km/hr, 100-160 km/hr, and the combined acceleration times, respectively. Note that the AP weighting factor q is set as 1.5 to give more weight to the low speed, which is generally used. Outstanding designs for the combined AP are spread along the diagonal line across the C1 and C1s regions where the engine and output nodes are located between the two EMs' nodes in the compound levers, with EM A and EM B located at roughly equal distances from the engine and the vehicle nodes, respectively. However, high α and β (spread ratio) do not necessarily lead to an optimal compound-split HEV design because the FE suffers when the selected values of α and β are too high as shown in Fig. 5. Therefore, a multi-objective configuration selection methodology is needed to find optimal compound-split HEV designs that simultaneously maximize and balance both the FE and AP.

IV. OPTIMAL CONFIGURATION SELECTION

In this section, a performance map is introduced to visualize and systematically compare the performance metrics of the 252 compound-split configurations. The design space conversion map is utilized to group the compound lever designs by configuration. Based on these clustered designs, an optimal compound-split configuration is selected.

A. PERFORMANCE MAP OF THE COMPOUND LEVER

In order to find the optimal compound-split configuration that has optimal FE and AP, the DP results are plotted onto a two-dimensional plane where the x-axis is FE and y-axis is acceleration time (i.e. AP). The FE and AP metrics are normalized as follows to compare the performance metrics in the same scale:

$$FE_{norm} = \left(\frac{FE_{min}}{FE_{design}}\right)^{r} \tag{8}$$

$$AT_{norm} = \left(\frac{AT_{design}}{AT_{max}}\right)^{s} \tag{9}$$

where FE_{norm} and AT_{norm} are normalized FE and acceleration time, respectively. Subscripts 'min' and 'max' refer to the minimum and maximum values of each performance metric, respectively, and 'design' is the corresponding design. Note that 'r' and 's' are the scaling factors of each performance metric. The two normalized performance metrics of all compound lever designs are plotted on the performance map as shown in Fig. 7. The black circles correspond to the performance of each POI in Section III. Since both performance metrics are normalized using Eq. (8) and Eq. (9), the designs located on the lower left corner are superior to other designs. The boundary line on the performance map shows the maximum reachable performance of compound-split HEVs for the given set of components listed in Table 4. Although optimal compound lever designs can be selected simply from the designs on this Pareto frontier, this approach may lead to configurations that are sensitive to changes of design variables. In other words, the performance of a configuration selected based on a single design point can rapidly deteriorate when its SR_{ratio}s or FD_{ratio} change. A robust optimal configuration must be selected based on the performance of multiple

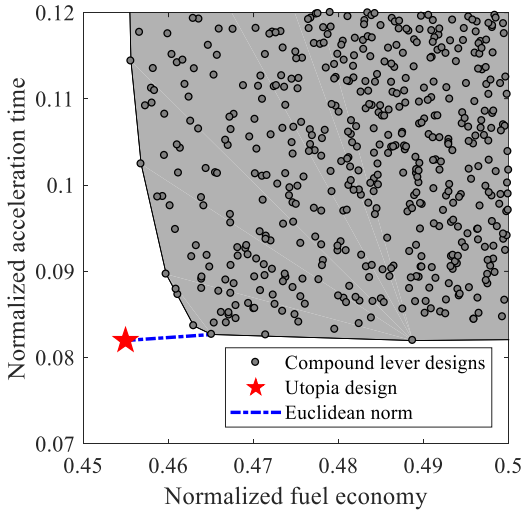

FIGURE 7. Performance map of compound-split HEVs.

designs for each configuration. Therefore, the potential of each configuration should be represented by a mathematical measure.

B. OPTIMAL CONFIGURATION SELECTION METHOD

First, a utopian (ideal) design is selected based on the minimum values of each performance metric (See Fig. 7). Designs located close to the utopian design will have outstanding performance. In order to quantify this optimality measure, the Euclidean norm of the utopian design and of each compound lever design is defined as follows:

$$d_k = \sqrt{w\left(FE_k - FE_{utopia}\right)^2 + (1-w)\left(AT_k - AT_{utopia}\right)^2}, \tag{10}$$

where w is the weighting factor, which adjusts the weighting ratio between the FE and acceleration time. In this study, to select an optimal configuration that balances both performance metrics, w is set as 0.5. Subscripts k and $utopia$ refer to the k_{th} design and the utopian design, respectively. The Euclidean norms of each compound lever design are grouped together by configuration using the design space conversion map. The Average Euclidean norm (AEN) of the 10 best designs (n = 10) is calculated using the following equation in order to compare the potential of the 252 configurations,

$$AEN = \frac{1}{n}\sum_{k=1}^{n} d_k. \tag{11}$$

The best 20 configurations are listed in Table 6. In terms of PG arrangements, PG arrangements #5, #11, #3, #9, #2, and #6 are used in the top 10 configurations, and in terms of components arrangements, components arrangements C1 and C1s are employed in the top 10 configurations. Note that the compound-split hybrid mode of the Volt 2nd generation is ranked 40, and there are many other configurations that are better than it. For more in-depth analyses, Fig. 8 shows the average Euclidean norms (AEN) of the 21 configurations using the C1 components arrangement combined with each of the 21 PG arrangements. Note that the smaller the AEN value of a configuration, the closer that configuration to the utopian design. Therefore, based on the results illustrated in Fig. 8, configurations #2-C1, #3-C1, #5-C1, #6-C1, #9-C1, and #11-C1 have high chances of being optimal configurations. Finally, the robustness of the highly ranked configurations is checked by comparing the Pareto frontier of each configuration. For instance, as illustrated in Fig. 9, configuration #5-C1 has a rounder shape of the Pareto frontier compared to configuration #3-C1s, which Pareto frontier has a sharper shape. This implies that configuration #5-C1 should be selected as the optimal compound-split configuration.

TABLE 6. Candidates of optimal compound-split HEV configuration.

Rank	Configuration	AEN*	Rank	Configuration	AEN
1	#5-C1	0.0278	12	#11-C4s	0.0589
2	#11-C1s	0.0281	13	#3-C4s	0.0633
3	#3-C1s	0.0303	14	#7-C4s	0.0654
4	#5-C1s	0.0312	15	#4-C4s	0.0670
5	#9-C1	0.0337	16	#9-C1s	0.0674
6	#2-C1	0.0401	17	#5-C4	0.0691
7	#6-C1	0.0401	18	#2-C1s	0.0695
8	#11-C1	0.0416	19	#5-C4s	0.0698
9	#3-C1	0.0461	20	#6r-C1	0.0702
10	#6-C1s	0.0553	:	:	:
11	#11-C4	0.0569	40	#6r-C1s (Volt 2nd)	0.1365

*AEN: Average Euclidean norm; lower value refers that a configuration locates closer to utopia.

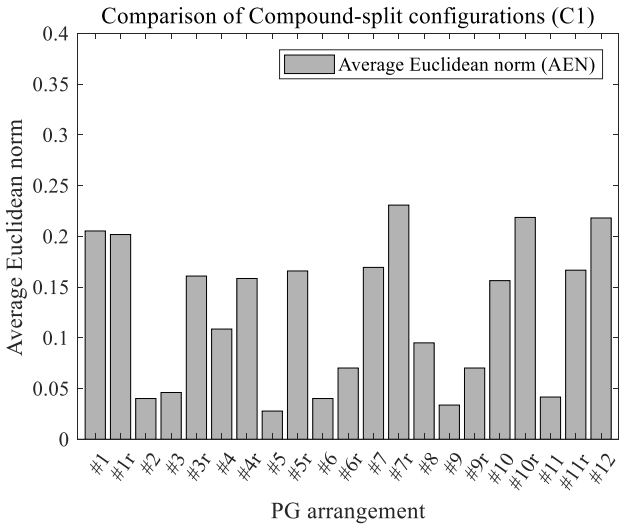

FIGURE 8. Comparison of compound-split configurations' average Euclidean norm; from "#1-C1" to "#12-C1" are provided as examples.

C. COMPARATIVE ANALYSIS OF SELECTED CONFIGURATIONS

The performance metrics of three configurations are compared based on their design space conversion maps. The red, green, and blue regions in Fig. 10 respectively represent the

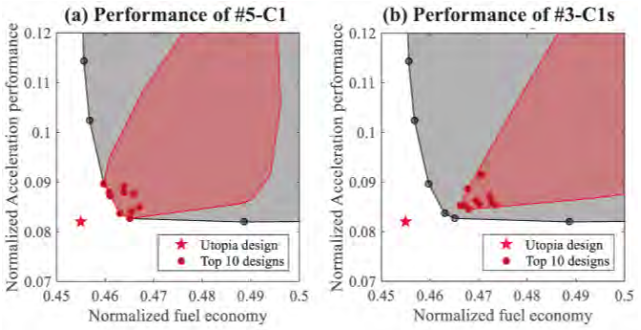

FIGURE 9. Performance maps of #5-C1 and #3-C1s.

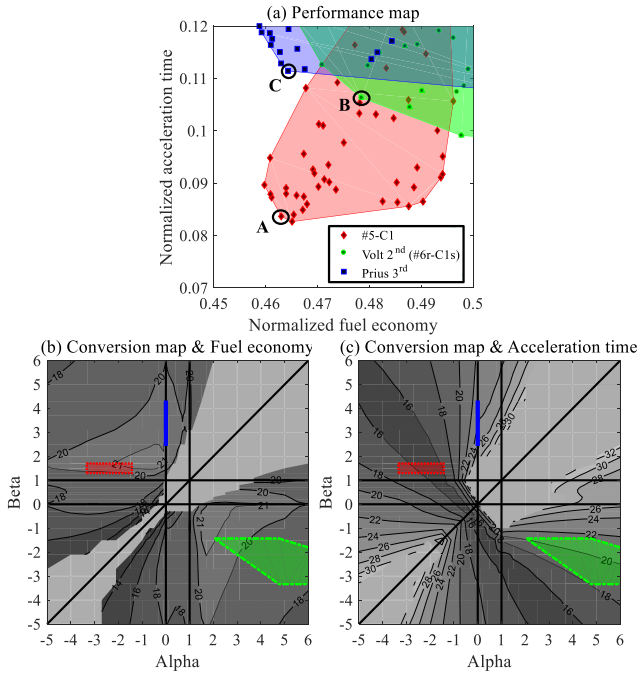

FIGURE 10. Performance map and design space conversion map of "#5-C1", Volt 2nd generation, Prius 3rd generation; A, B, and C are the optimal design of each configuration.

conversion maps of the selected optimal configuration (i.e. #5-C1) and two commercialized configurations: compound-split mode of Volt 2nd generation (i.e. #6r-C1s) and Prius 3rd generation (i.e. an input-split with torque multiplication gear). As illustrated in Fig. 10 (b) and (c), the feasible region of the selected optimal configuration #5-C1 is located on the high FE and low acceleration time region. Thus, #5-C1 outperforms the other two configurations. For further comparative analysis, optimal designs A, B, and C, which are illustrated in Fig. 10 (a), are selected as the best designs of each configuration.

The design variables, configuration, and performance metrics of these three designs are summarized in Table 7. The FEs of these three configurations are comparable with that of the new configuration found in this study (i.e. #5-C1) slightly better than the other two configurations. On the other hand, the acceleration time of #5-C1 is much shorter than those of the other two configurations, which implies that #5-C1 has the fastest acceleration performance.

TABLE 7. Comparison between optimal compound-split HEV designs.

Optimal Design	A	B	C
α	-2.1	2.5	0
β	1.7	-1.5	4.33
Speed reduction gear (SRG)	-	-	1.43
Configuration	#5-C1	#6r-C1s (Voltec 2nd)	Prius 3rd
Elementary Lever Representation	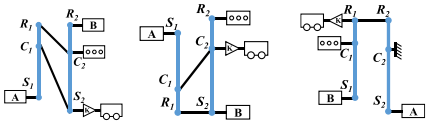		
$SR_{1,ratio}$	0.48	0.60	0.3
$SR_{2,ratio}$	0.70	0.67	0.7
FD_{ratio}	4	4.5	4.5
City FE [km/liter]	21.13	21.37	22.55
Highway FE [km/liter]	20.95	19.64	19.92
Combined FE [km/liter]	21.03	20.35	20.97
0-100 kph time [sec]	7.37	8.72	9.42
100-160 kph time [sec]	7.99	12.09	11.84
Combined acceleration time [sec]	15.05	19.13	20.05

For a more in-depth comparison, the battery state of charge, accumulated fuel consumption, vehicle tractive force, vehicle velocity, and operating points of the selected designs are plotted in Fig. 11. As observed in the operating points for the UDDS driving cycle, the engine operations of all three designs are concentrated in the minimum brake specific fuel consumption region, whereas the EM A and EM B operations are quite different. Despite various EM operations, the fuel consumptions of the three configurations are quite similar. On the other hand, the operations of EM A and EM B for the acceleration performance significantly affect the vehicle tractive force and launching performance. Figure 11 shows that both EM A and EM B of configuration #5-C1 consistently produce the maximum motoring torque (power), whereas the two EMs of the other two configurations sometimes do not produce their full power, which results in a lower tractive force. The different operating characteristic of each configuration comes from the different lever length. Only the optimal selected design variables (α and β) enable powertrain components to produce their full potential. In contrast, a specific length of α or β can even make the powertrain infeasible. This problem results from the speed, torque, or power constraints of each component. Therefore, in order to find the optimal compound-split configuration and its corresponding design variables, the entire compound-split HEV design space was exhaustively evaluated in terms of both the FE and the AP.

Finding a novel good performing configuration (i.e. #5-C1) proves that a full systematic design space search is highly required to find globally optimal configuration, and that relying on experience, insights, and simple (static) analysis tools, which the authors believe to be a common practice in industry, is not enough. Furthermore, assessing the performance within the virtual design space is not only efficient because it dramatically reduces the design space, but

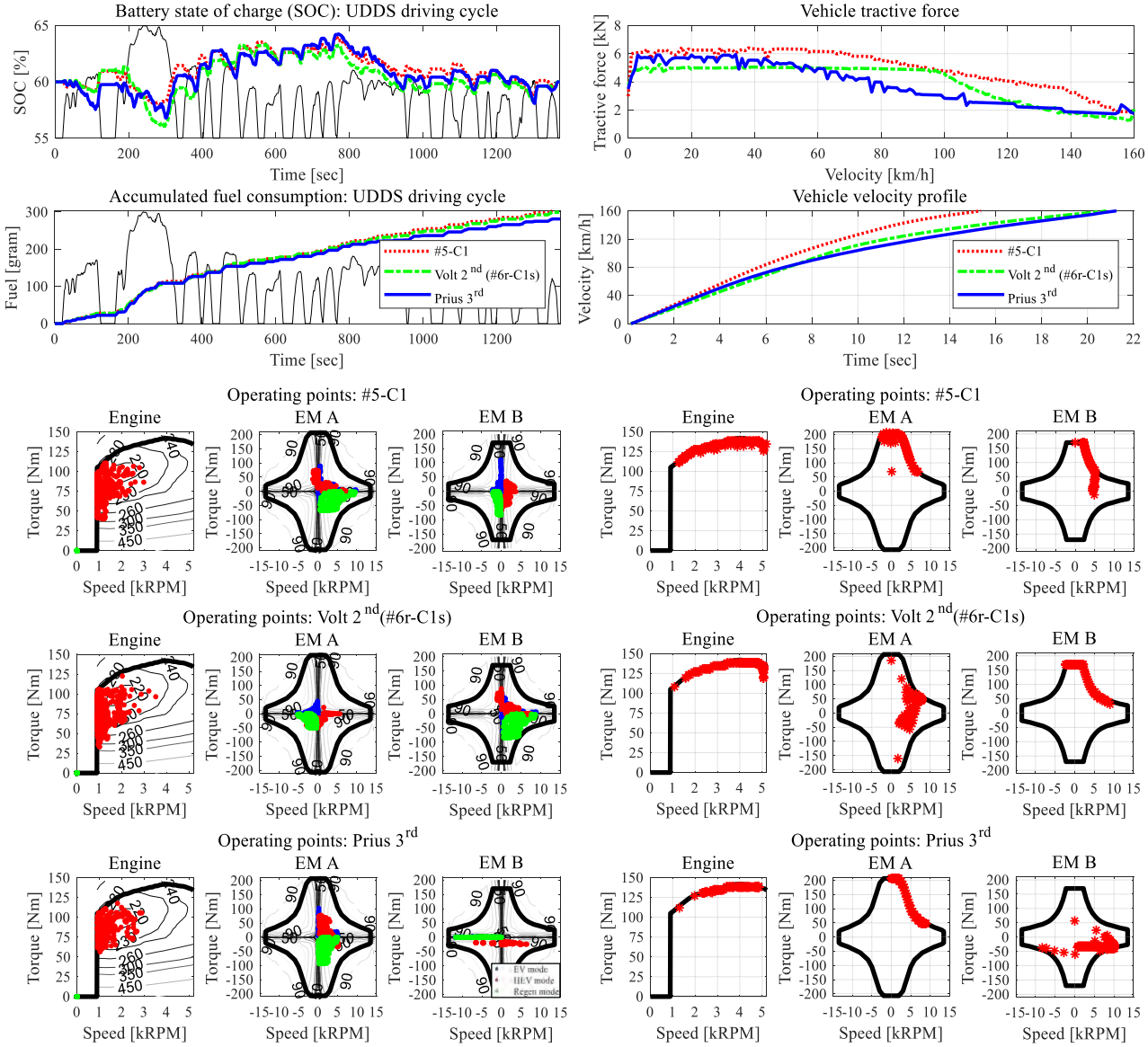

FIGURE 11. Operating characteristics of selected configurations: Battery state of charge, fuel consumption, and operating points plot for fuel economy assessment, and vehicle tractive force, velocity response, and operating points plot for acceleration performance assessment.

it also provides insights at a glance on how the performance of a given configuration changes as its design variables change (See Figures 5, 6, and 10).

Despite its optimal performance metrics, the configuration "#5-C1" cannot be implemented unless it is depicted (i.e. its kinematic diagrams are generated). In fact, the kinematic diagrams are required not only to check its possible realization, but also to verify the physical constraints [37]. The systematic generation of feasible kinematic diagrams for compound-split hybrid configurations is the future work of this study.

V. CONCLUSION

This paper proposed a compound lever-based split hybrid configuration search methodology that enables the full design domain search with dramatically reduced computational load. First, both fuel economy and acceleration time are assessed in the virtual compound lever design space rather than the physical design space of the compound-split HEVs in order to avoid redundant performance assessments and to observe the performance trends in the abstracted design space. These two performance metrics calculated for all split HEV designs are plotted onto the 2-dimensional plane with the normalized fuel economy and normalized acceleration performance as its axes. Compound lever designs on the performance map are grouped together according to each compound-split configuration using the design space conversion map so that the performance of the 252 compound-spilt HEVs can be systematically compared. As a result, many new promising configurations are found in this study, and configuration #5-C1 is selected as the robust optimal compound-split configuration.

This configuration shows dramatically improved acceleration performance compared to that of Prius 3rd and Volt 2nd generations powertrains assuming that the same components are used. Despite its high performance, the selected configuration cannot be directly implemented since additional constraints should be considered through their kinematic diagrams. The systematic depiction of compound-split configurations is the future work of this study.

APPENDIX A

Fig. 12 shows the 21 planetary gear arrangements.

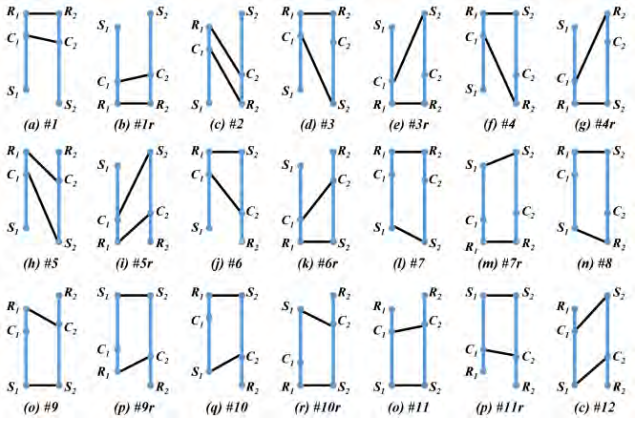

FIGURE 12. 21 PG arrangements with two elementary levers.

APPENDIX B

Fig. 13 shows the 12 components arrangements.

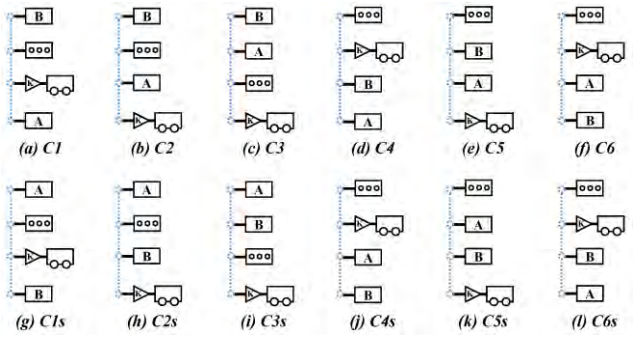

FIGURE 13. 12 component arrangements of compound-split configuration.

ACKNOWLEDGMENT

(Hyunjun Kim and Toumadher Barhoumi are co-first authors.)

REFERENCES

[1] V. Freyermuth, E. Fallas, and A. Rousseau, "Comparison of powertrain configuration for plug-in HEVs from a fuel economy perspective," *SAE Int. J. Engines*, vol. 1, no. 1, pp. 392–398, Jan. 2009.

[2] T. Barhoumi, H. Kim, and D. Kum, "Automatic generation of design space conversion maps and its application for the design of compound split hybrid powertrains," *J. Mech. Des.*, vol. 140, no. 6, Mar. 2018, Art. no. 063401.

[3] H. Kim and D. Kum, "Comprehensive design methodology of input- and output-split hybrid electric vehicles: In search of optimal configuration," *IEEE/ASME Trans. Mechatronics*, vol. 21, no. 6, pp. 2912–2923, Dec. 2016.

[4] A. E. Bayrak, Y. Ren, and P. Y. Papalambros, "Optimal dual-mode hybrid electric vehicle powertrain architecture design for a variety of loading scenarios," in *Proc. Int. Des. Eng. Tech. Conf. Comput. Inf. Eng. Conf.*, Aug. 2014, Art. no. V003T01A005.

[5] D. E. Kirk, *Optimal Control Theory*. Englewood Cliffs, NJ, USA: Prentice-Hall, 1970, pp. 53–93.

[6] D. Bertsekas, *Dynamic Programming and Optimal Control*. Boston, MA, USA: Athena Scientific, 2000, pp. 2–50.

[7] H. Yang, S. Cho, N. Kim, W. Lim, and S. Cha, "Analysis of planetary gear hybrid powertrain system part 1: Input split system," *Int. J. Automot. Technol.*, vol. 8, no. 6, pp. 771–780, 2007.

[8] H. Yang, B. Kim, Y. Park, W. Lim, and S. Cha, "Analysis of planetary gear hybrid powertrain system part 2: Output split system," *Int. J. Automotive Technol.*, vol. 10, no. 3, pp. 381–390, 2009.

[9] S.-H. Yuan, H. Liu, Z.-X. Peng, and B. Wei, "Analysis of the compound split transmission based on the four-port power split device," *J. Beijing Inst. Technol.*, vol. 21, no. 1, pp. 50–57, Mar. Mar. 2012.

[10] B. Conlon, "Comparative analysis of single and combined hybrid electrically variable transmission operating modes," in *Proc. SAE Trans.*, Vol. 114, 2005, pp. 1265–1275.

[11] W. Wang, R. Song, M. Guo, and S. Liu, "Analysis on compound-split configuration of power-split hybrid electric vehicle," *Mechanism Mach. Theory*, vol. 78, pp. 272–288, Aug. 2014.

[12] K. L. Cheong, P. Y. Li, S. Sedler, and T. R. Chase, "Comparison between input coupled and output coupled power-split configurations in hybrid vehicles," in *Proc. 52nd Nat. Conf. Fluid Power, Nat. Fluid Power Assoc.*, Mar. 2011, pp. 53219–53222.

[13] K. L. Cheong, P. Y. Li, and T. R. Chase, "Optimal design of power-split transmissions for hydraulic hybrid passenger vehicles," in *Proc. ACC*, Jun./Jul. 2011, pp. 3295–3300.

[14] A. T. Zaremba, C. Soto, and M. Jennings, "Methodology for assessment of alternative hybrid electric vehicle powertrain system architectures," *SAE Int. J. Alternative Powertrains*, vol. 1, no. 1, pp. 1–10, Jun. 2012.

[15] H. Kim, J. Kang, and D. Kum, "Impact of speed reduction (multiplication) gear on the performance of input- and output-split hybrid electric vehicles," in *Proc. SAE World Congr. Exper.*, 2017.

[16] Z. Qin, Y. Luo, W. Zhuang, Z. Pan, K. Li, and H. Peng, "Simultaneous optimization of topology, control and size for multi-mode hybrid tracked vehicles," *Appl. Energy*, vol. 212, pp. 1627–1641, Feb. 2018.

[17] J. Liu and H. Peng, "A systematic design approach for two planetary gear split hybrid vehicles," *Vehicle Syst. Dyn.*, vol. 48, no. 11, pp. 1395–1412, Oct. 2010.

[18] C.-T. Li, X. Zhang, and H. Peng, "Design of power-split hybrid vehicles with a single planetary gear," in *Proc. 5th Annu. Dyn. Syst. Control Conf. Joint JSME, 11th Motion Vib. Conf.*, Oct. 2012, pp. 857–865.

[19] W. Zhuang, X. Zhang, H. Peng, and L. Wang, "Rapid configuration design of multiple-planetary-gear power-split hybrid powertrain via mode combination," *IEEE/ASME Trans. Mechatronics*, vol. 21, no. 6, pp. 2924–2934, Dec. 2016.

[20] X. Zhang, S. E. Li, H. Peng, and J. Sun, "Efficient exhaustive search of power-split hybrid powertrains with multiple planetary gears and clutches," *J. Dyn. Syst., Meas., Control*, vol. 137, no. 12, Sep. 2015, Art. no. 121006.

[21] X. Zhang, S. E. Li, H. Peng, and J. Sun, "Design of multimode power-split hybrid vehicles—A case study on the voltec powertrain system," *IEEE Trans. Veh. Technol.*, vol. 65, no. 6, pp. 4790–4801, Jun. 2016.

[22] X. Zhang, H. Peng, and J. Sun, "A near-optimal power management strategy for rapid component sizing of multimode power split hybrid vehicles," *IEEE Trans. Control Syst. Technol.*, vol. 23, no. 2, pp. 609–618, Mar. 2015.

[23] K. Ahn, S. Cho, W. Lim, Y.-I. Park, and J. M. Lee, "Performance analysis and parametric design of the dual-mode planetary gear hybrid powertrain," *Proc. Inst. Mech. Eng., D, J. Automobile Eng.*, vol. 220, no. 11, pp. 1601–1614, Nov. 2006.

[24] A. E. Bayrak, Y. Ren, and P. Y. Papalambros, "Design of hybrid-electric vehicle architectures using auto-generation of feasible driving modes," in *Proc. Int. Des. Eng. Tech. Conf. Comput. Inf. Eng. Conf.*, Aug. 2013, Art. no. V001T01A005.

[25] H. L. Benford and M. B. Leising, "The lever analogy: A new tool in transmission analysis," in *Proc. SAE Trans.*, vol. 90, 1981, pp. 429–437.

[26] A. E. Bayrak, Y. Ren, and P. Y. Papalambros, "Topology generation for hybrid electric vehicle architecture design," *J. Mech. Des.*, vol. 138, no. 8, 2016, Art. no. 081401.
[27] H. Ngo and H. Yan, "Configuration synthesis of series-parallel hybrid transmissions," *Proc. Inst. Mech. Eng., D, J. Automobile Eng.*, vol. 230, no. 5, pp. 664–678, 2016.
[28] J. Liu, H. Peng, and Z. Filipi, "Modeling and analysis of the toyota hybrid system," in *Proc. IEEE/ASME Int. Conf. Adv. Intell. Mechatronics*, Jul. 2005, pp. 134–139.
[29] J. Liu and H. Peng, "Modeling and control of a power-split hybrid vehicle," *IEEE Trans. control Syst. Technol.*, vol. 16, no. 68, pp. 1242–1251, Nov. 2008.
[30] Argonne National Laboratory. *Downloadable Dynamometer Database*. Accessed: Jul. 2, 2019. [Online]. Available: https://www.anl.gov/es/energy-systems-d3-2010-toyota-prius
[31] K. Muta, M. Yamazaki, and J. Tokieda, "Development of new-generation hybrid system THS II—drastic improvement of power performance and fuel economy," in *Proc. SAE World Congr. Exhib.*, 2004.
[32] A. Rousseau, J. Kwon, P. Sharer, S. Pagerit, and M. Duoba, "Integrating data, performing quality assurance, and validating the vehicle model for the 2004 prius using PSAT," in *Proc. SAE World Congr. Exhib.*, 2006.
[33] A. Sundström, L. Guzzella, and P. Soltic, "Optimal hybridization in two parallel hybrid electric vehicles using dynamic programming," in *Proc. 17th World Congr. Int. Fed. Autom. Control*, Jul. 2008, pp. 4642–4647.
[34] G. Paganelli, S. Delprat, T. M. Guerra, J. Rimaux, and J. J. Santin, "Equivalent consumption minimization strategy for parallel hybrid powertrains," in *Proc. IEEE 55th Veh. Technol. Conf. (VTC Spring)*, May 2012, pp. 2076–2081.
[35] X. Zhang, H. Peng, and J. Sun, "A near-optimal power management strategy for rapid component sizing of multimode power split hybrid vehicles," *IEEE Trans. Control Syst. Technol.*, vol. 23, no. 2, pp. 609–618, Mar. 2015.
[36] Office of Transportation and Air Quality of United States Environmental Protection Agency, "Final technical support document fuel economy labeling of motor vehicle revisions to improve calculation of fuel economy estimates," United States Environ. Protection Agency, Washington, DC, USA, Tech. Rep. EPA420-R-06-017, 2006.
[37] T. Barhoumi and D. Kum, "Automatic enumeration of feasible kinematic diagrams for split hybrid configurations with a single planetary gear," *J. Mech. Des.*, vol. 139, no. 8, May 2017, Art. no. 083301.

HYUNJUN KIM received the master's degree from the Korea Advanced Institute of Science and Technology (KAIST), Daejeon, South Korea, in 2015, where he is currently pursuing the Ph.D. degree. His current research interest includes design optimization of the input-, output-, and compound-split HEVs.

TOUMADHER BARHOUMI received the bachelor's and master's degrees from the Korea Advanced Institute of Science and Technology (KAIST), Daejeon, South Korea, in 2014 and 2017, respectively, where she is currently pursuing the Ph.D. degree. Her research interest includes the design and control of hybrid electric vehicles.

DONGSUK KUM received the Ph.D. degree in mechanical engineering from the University of Michigan, Ann Arbor, MI, USA, in 2010.

He is currently an Associate Professor with the Graduate School of Green Transportation, Korea Advanced Institute of Science and Technology (KAIST), and the Director of the Vehicular System Design and Controls (VDC) Laboratory. Prior to joining KAIST, he had worked for the General Motors R&D Propulsion Systems Research Laboratory, Warren, MI, USA, as a Visiting Research Scientist. His works at General Motors focused on advanced propulsion system technologies, including hybrid electric vehicles, flywheel hybrid, and waste heat recovery systems. His research centers on the modeling, control, and design of advanced vehicular systems, with particular interests in hybrid electric vehicles and autonomous vehicles.